# Elevated Proton Leak of the Intermediate $O_H$ in Cytochrome *c* Oxidase

Dmitry A. Bloch, Audrius Jasaitis, and Michael I. Verkhovsky*
Institute of Biotechnology, 00014 University of Helsinki, Helsinki, Finland

ABSTRACT The kinetics of the formation and relaxation of transmembrane electric potential ($\Delta\psi$) during the complete single turnover of C*c*O was studied in the bovine heart mitochondrial and the $aa_3$-type *Paracoccus denitrificans* enzymes incorporated into proteoliposome membrane. The real-time $\Delta\psi$ kinetics was followed by the direct electrometry technique. The prompt oxidation of C*c*O and formation of the activated, oxidized ($\mathbf{O_H}$) state of the enzyme leaves the enzyme trapped in the open state that provides an internal leak for protons and thus facilitates dissipation of $\Delta\psi$ ($\tau^{app} \leq 0.5$–$0.8$ s). By contrast, when the enzyme in the $\mathbf{O_H}$ state is rapidly re-reduced by sequential electron delivery, $\Delta\psi$ dissipates much slower ($\tau^{app} > 3$ s). In *P. denitrificans* C*c*O proteoliposomes the accelerated $\Delta\psi$ dissipation is slowed down by a mutational block of the proton conductance through the D-, but not K-channel. We concluded that in contrast to the other intermediates the $\mathbf{O_H}$ state of C*c*O is vulnerable to the elevated internal proton leak that proceeds via the D-channel.

## INTRODUCTION

C*c*O is the terminal enzyme of the respiratory chain in mitochondria and aerobic bacteria. C*c*O accepts four electrons from the reduced cytochrome *c* and catalyses reduction of dioxygen to two water molecules. This reaction is highly exergonic and the released energy is conserved by the enzyme in the form of electrochemical proton gradient across the membrane ($\Delta\tilde{\mu}_{H^+}$) (1). The chemical component of $\Delta\tilde{\mu}_{H^+}$ ($\Delta$pH) accumulates when a $\Delta\tilde{\mu}_{H^+}$-generator operates in a continuous turnover regime. In presteady-state (e.g., when a single turnover of the enzyme is followed in a transient kinetics experiment) $\Delta\tilde{\mu}_{H^+}$ is present in its primary electrical component (transmembrane electric potential, $\Delta\psi$). Two mechanisms contribute to the $\Delta\psi$ generation by C*c*O: 1), ''vectorial'' chemistry, and 2), proton pumping. In the first mechanism the extent of $\Delta\psi$ generation is determined by the spatial distribution of the charge-transporting groups within the enzyme dielectric. Electrons enter C*c*O via soluble cytochrome *c* from the *P*-side of the membrane while protons to form water are taken up from the N-side; this process contributes altogether to the transfer of four net charges across the membrane per turnover (2). In addition, C*c*O is a proton pump (3): for each molecule of oxygen bound, four more protons are translocated across the membrane, making the overall stoichiometry of eight net transmembrane charges per enzyme turnover.

The catalytic cycle of C*c*O is often described as a sequence of states of the enzyme's oxygen-binding heme $a_3$–$Cu_B$ catalytic center (BNC), which receives one electron at a time from cytochrome *c* via two one-electron metal centers $Cu_A$ and heme *a*. The catalytic cycle is divided into two half-reactions. In the oxidative half-reaction, reduced BNC (state **R**) binds oxygen and reduces it with four electrons, two of which are taken from the reduced heme *a* and $Cu_A$, to form water and to get to fully oxidized state ($\mathbf{O_H}$) through a number of well-defined intermediates (states **A**, **P**, and **F**) (4,5). In the reductive half-reaction the freshly oxidized BNC successively receives two electrons ($\mathbf{O_H} \rightarrow \mathbf{E_H} \rightarrow \mathbf{R}$) to complete the cycle. However, two more electrons are required to reduce heme *a* and $Cu_A$ to return into initial state $\mathbf{R_{FR}}$. In the continuous turnover regime four protons are pumped during the whole cycle, one proton at each reduction step of BNC, that is, two protons at each of the oxidative ($\mathbf{R} \rightarrow \mathbf{O_H}$) and the reductive ($\mathbf{O_H} \rightarrow \mathbf{R}$) phase (6,7). This differs from the situation when the reduction has not been preceded immediately by oxidation, when no proton pumping accompanies the reduction. The difference has been ascribed to the properties of special ''freshly-oxidized'' state $\mathbf{O_H}$ as opposed to the ''as prepared'', inactive oxidized state **O** (8,9). In the meantime, the state $\mathbf{O_H}$ has not been yet well characterized and requires more study.

We have shown earlier that the oxidative and reductive parts of the C*c*O catalytic cycle can be kinetically separated (6). In this study we address the question about possible different proton leak specificity in different catalytic states of C*c*O is also taken into account.

*Submitted December 3, 2008, and accepted for publication March 11, 2009.*

*Correspondence: michael.verkhovsky@helsinki.fi

Audrius Jasaitis's present address is Institut Curie, 26 rue d'Ulm, 75248 Paris, France.

*Abbreviations used:* BNC, heme-copper binuclear center of cytochrome *c* oxidase; C*c*O, cytochrome *c* oxidase; **E**, one electron-reduced binuclear center; $\mathbf{E_H}$, freshly formed, one electron-reduced binuclear center; EPPS, *N*-(2-hydroxyethyl)piperazine-*N*′-(3-propanesulfonic acid); **F**, oxoferryl binuclear center; GO, glucose oxidase; HAR, hexaammineruthenium; **O**, fully oxidized binuclear center; $\mathbf{O_H}$, freshly formed, activated fully oxidized binuclear center; **P**, peroxy binuclear center; **R**, two-electron-reduced binuclear center; $\mathbf{R_{FR}}$, two-electron-reduced binuclear center of the fully reduced cytochrome *c* oxidase; **RCO**, two-electron-reduced binuclear center with a bound carbon monoxide molecule; WT, wild-type; $\Delta\tilde{\mu}_{H^+}$, transmembrane electrochemical proton gradient; $\Delta\Psi$, transmembrane difference of electric potential; $\Psi$, number of electrogenically transferred charges.

Editor: Janos K. Lanyi.


0006-3495/09/06/4733/10 $2.00

doi: 10.1016/j.bpj.2009.03.006

## MATERIALS AND METHODS

### Reagents and materials

All chemicals were of ACS or higher grade from Sigma-Aldrich Finland Oy (Helsinki, Finland) unless otherwise stated. Gases were from Linde Gas/AGA (Enköping, Sweden). Double-deionized water was used throughout the experiments.

Direct, time-resolved electrometry is based on the technique introduced by Drachev et al. (10,11) and further developed in our laboratory (12,13). In this setup voltage changes across the measuring phospholipid film were recorded using a pair of fretted, light-shielded Ag/AgCl electrodes (Dri-Ref 5SH, World Precision Instruments, Sarasota, FL) filled with 3 M KCl, amplified using a broad-band, high input-impedance Burr-Brown 3554BM amplifier (Texas Instruments, Dallas, TX), and digitized with a GaGe plug-in ADC board (GaGe Applied Technologies, Lockport, IL). The measuring film was prepared by heating and stretching out plumber's tape made of porous Teflon (75 $\mu$m-thick Unitape, Unipak A/S, Brabrand, Denmark). The thin micromesh obtained was impregnated with the solution of asolectin (soybean phospholipids, phosphatidylcholine type II-S, 100 mg/mL) in *n*-decane (Fluka, Sigma-Aldrich Finland Oy, Helsinki, Finland) and pressed between two Teflon compartments, each filled with 800 $\mu$L of an electrolyte, of a sample assembly. The film surface was partly exposed to the electrolyte through the circular opening (diameter 4 mm, area ~12.5 $mm^2$) in each compartment. Phospholipid vesicles (proteoliposomes with the membrane-reconstituted C*c*O) were attached to the electrolyte-exposed surface of the measuring film at one side by means of divalent cation-induced lipid membrane fusion (14,15) that ensures common lipid phase to form between the measuring film and the attached proteoliposomes. As a result, a monolayer of membrane-embedded, immobilized C*c*O is produced at one side of the film. The recorded voltage between the two compartments is proportional to the $\Delta\psi$ changes across the proteoliposome membrane over a broad frequency range, which allows one to follow the real-time electrogenic charge translocation within the reconstituted enzyme (see Hendler et al. (16), Schönfeld et al. (17), and Gopher et al. (18) for measurement principles and theory). Each sample assembly was placed into a vacuum/gas-tight box (internal volume, 480 mL, see below) and mounted into an electrostatically-shielded cage with the access of a laser beam to the measuring film. Photolysis of the carbon monoxide (CO) adduct of the fully reduced C*c*O in the attached proteoliposomes was initiated by the pulses of a frequency-doubled, Q-switched Nd-YAG laser (Brilliant-B, pulse width 4 ns, $\lambda = 532$ nm; Quantel, Les Ulis, France). The laser beam was focused so that the illuminated spot covered ~90% of the exposed part of the measuring film. A 0.8 J/$cm^2$ pulse caused ~99% saturation of the CO photolysis yield. The time resolution of the setup was ~0.1 $\mu$s.

### Sample preparation

Site-directed mutagenesis of *Paracoccus denitrificans* C*c*O was accomplished as in (19). The $aa_3$-type C*c*O from bovine heart mitochondria (20), or *P. denitrificans* cells (21,22) was isolated and purified, as indicated. C*c*O-containing proteoliposomes (7 $\mu$M enzyme and 80 mg/mL lipid) were prepared as in Jasaitis et al. (13) using a procedure based on formation of the mixed enzyme-lipid-sodium cholate (2%, w/v) micelles followed by the slow, stepwise removal of the detergent by Bio-Beads SM-2 adsorbent (Bio-Rad, Hercules, CA) (23). Proteoliposomes were incubated with 20 mM $MgSO_4$ in one of the two compartments of a sample assembly for 2–3 h; then the buffer with unattached proteoliposomes were replaced with fresh buffer (100 mM EPPS, pH 8.1) containing 100 mM D-glucose, glucose oxidase (GO) at various concentration (type X-S, see below), and 0.2 mg/mL catalase. Oxidized hexaammineruthenium ($HAR^{Ox}$, 0.05 $\mu$M–5 mM) was added when necessary. The glucose-GO-catalase enzymatic system ensured that 1), dissolved oxygen is efficiently depleted from the sample; 2) C*c*O is fully reduced in the preflash state; 3), redox mediator, if present, is reduced in equilibrium (see Supporting Material). Particularly, in the presence of the GO, $HAR^{Ox}$ is converted to the reduced form ($HAR^{Red}$) serving as a rapid reductant to C*c*O. The atmosphere inside the vacuum/gas-tight box with a sample assembly was repeatedly exchanged with Ar gas (99.9999%) followed by carbon monoxide (99.99%). Typically, it took from 10 min to 2 h to fully deplete traces of oxygen and reduce C*c*O, depending both on the concentration of GO and $HAR^{Red}$. The reduction state of C*c*O was checked in situ by the lack of the electrometric electron backflow kinetics on CO photolysis, which is only observed when the enzyme is in the two- or three electron-reduced mixed valence state and that disappears in the fully reduced C*c*O (13), and by the appearance of a very fast ($\tau$, 1–2 $\mu$s), small electrogenic phase ($\Delta\psi_{CO}$; see Results) specific to the CO photolysis from the fully reduced enzyme. During the experiment additions to the sample were made through a low-bleed rubber septum (Hamilton Company, Reno, NV) using a gas-tight Hamilton syringe. The samples were kept under the CO atmosphere continuously stirred throughout the experiments. The measurements were carried out at +21°C.

### Electrometric flow-flash measurements

In the flow-flash experiment, the fully reduced, $\mathbf{R_{FR}}$-state C*c*O is instantaneously liberated after the photolysis of the C*c*O-CO adduct to bind oxygen and reduce it within 3–5 ms (oxidative half-reaction). Because in the dark state, oxygen (1.2 mM, $O_2$-saturated aqueous solution at 1.013 bar and +21°C) competes with CO to bind to C*c*O, it should be delivered to the system promptly before the photolysis. A computer-driven syringe pump (World Precision Instruments) was used to inject 40 $\mu$L of oxygen-saturated buffer into the sample compartment (800 $\mu$L) at the speed 80 $\mu$L/s. The jet from the needle was directed at the measuring film on one side to produce an oxygen-enriched space around the immobilized C*c*O while mixing was turned off. Immediately after injection, when the local concentration of oxygen is the maximum, a laser flash initiated CO photolysis. After the oxidative phase is complete, C*c*O is trapped in the oxidized state, $\mathbf{O_H}$, until it becomes slowly re-reduced ($\tau^{obs} >> 10$ s, 0.05–0.2 $\mu$M $HAR^{Red}$) when it can bind CO to return to the initial state (Scheme 1). High concentration of GO (200 U/mL, 1.2-1.4 mg/mL $\approx$ 8-10 $\mu$M) was used to rapidly consume the injected oxygen after the oxygen-induced reaction had been recorded and when mixing in the sample was turned on again. Under such conditions multiple turnover of the enzyme is prevented by very small concentration of electron donor so that $\Delta\psi$ relaxation kinetics on state $\mathbf{O_H}$ formation can be followed.

### Electrometric complete single turnover measurements

To follow both oxidative and reductive half-reactions of C*c*O in one experiment, it is prerequisite that after oxidation C*c*O is rapidly re-reduced with an electron donor. Therefore, very little amount of oxygen should be present so that its slow binding after one turnover would not lead to any substantial subsequent turnover. For this purpose the CO atmosphere also contained ~0.1% (v/v) air, which ensured constant influx of oxygen into the bulk solution of a sample. GO (12–16 U/mL, 0.08–0.1 mg/mL $\approx$ 0.5–0.6 $\mu$M) was used to slowly consume the incoming oxygen so that its very low steady-state concentration is maintained at the measuring film surface. The exact concentration of oxygen can be found from the observed flash-induced kinetics, as follows. When both CO and oxygen are present, CO photolysis allows C*c*O either to re-bind CO or react with oxygen (Scheme 1). Conversion of the state $\mathbf{R_{FR}}$ into the products ($\mathbf{R_{FR}CO}$ or $\mathbf{O_H}$) is described by a one-exponent kinetics, where its apparent rate constant is a sum of the apparent rate constants for the two parallel irreversible reactions:

$$k_1^{app} = k_{on}^{CO} \times [CO] + k_{on}^{O_2} \times [O_2]. \quad (1)$$

The molar fraction $\alpha$ of C*c*O found in the state $\mathbf{O_H}$ when the reaction is complete, is given by

$$\alpha = \frac{k_{on}^{O_2} \times [O_2]}{k_{on}^{O_2} \times [O_2] + k_{on}^{CO} \times [CO]}. \quad (2)$$

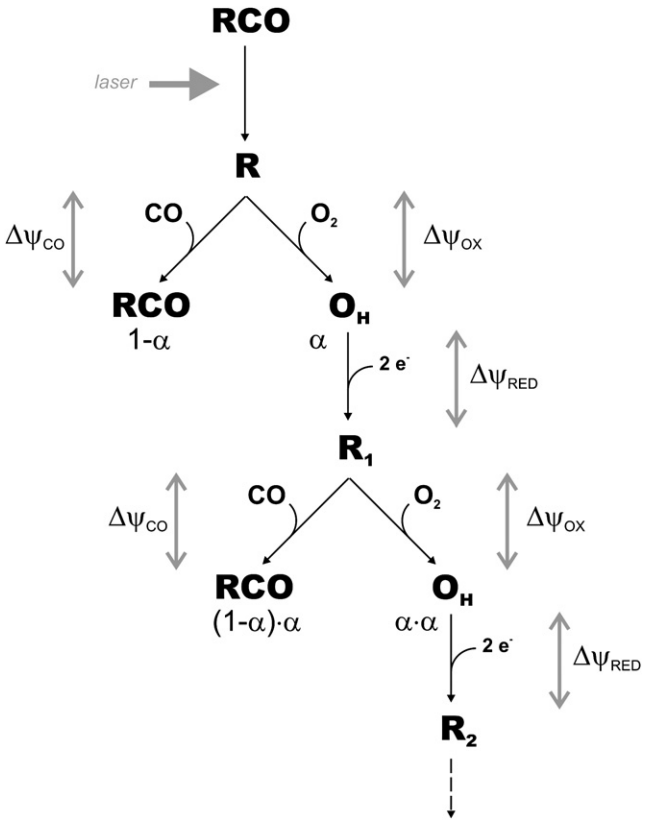


SCHEME 1 Membrane potential generation in C*c*O-proteoliposomes after the laser flash-induced photolysis of C*c*O-CO complex. Voltage associated with the oxidative and reductive phases of the catalytic cycle and re-binding of CO is denoted as $\Delta\psi_{OX}$, $\Delta\psi_{RED}$, and $\Delta\psi_{CO}$, respectively.

At [CO] $\approx$ 950 $\mu$M (100% CO-saturated aqueous solution at 1.013 bar and +21°C) $k_{on}^{CO} \times [CO] = 44s^{-1}$ (*Paracoccus* C*c*O (24)) and $k_{on}^{O_2} = 1.4 \times 10^7$ $M^{-1}s^{-1}$ (the only available literature data are for the bovine mitochondrial enzyme (25,26)), which gives $[O_2] = 3.1 \times 10^{-6} \times \frac{\alpha}{1-\alpha}$ M (Eq. 2). With $k_{on}^{CO} \times [CO] = 60s^{-1}$ (bovine mitochondrial enzyme (27)) the value is $4.3 \times 10^{-6} \times \frac{\alpha}{1-\alpha}$ M. When $\alpha << 0.5$ ($[O_2] << 3\text{-}4 \times 10^{-6}$ M) CO binding prevails, so that

$$k_1^{app} \cong k_{on}^{CO} \times [CO]. \tag{3}$$

Note that the same constant $k_1^{app}$ describes both binding of CO and reaction with $O_2$ and, therefore, the kinetics of $\Delta\psi$ generation during the oxidative phase ($\Delta\psi_{OX}$). The value of $\alpha$ can be found independently from the experiment as the ratio between the amplitudes of $\Delta\psi_{OX}$ measured in the flow-flash experiment ($\Delta\psi_{OX}^{100\%}$, reflecting 100% of C*c*O) and complete single turnover experiment with the same sample ($\Delta\psi_{OX}^{\alpha}$, reflecting a small fraction of C*c*O):

$$\alpha = \frac{\Delta\psi_{OX}^{\alpha}}{\Delta\psi_{OX}^{100\%}}. \tag{4}$$

For example, in Figs. 2 and 3 $\Delta\psi_{OX}^{100\%} \approx 100$ mV, $\Delta\psi_{OX}^{\alpha} \approx 2$ mV, and $\alpha = 0.02$, which gives steady-state $[O_2] \approx 63$ nM (*Paracoccus* enzyme). For the range of $\alpha \cong 0.01$–$0.05$ typically observed in the experiments, $[O_2] \approx$ 30–160 nM. For bovine enzyme, $\alpha = 0.02$ gives $[O_2] = 88$ nM. In the presence of the reductant the oxidized fraction of the enzyme is re-reduced generating $\Delta\psi_{RED}^{\alpha}$. After the re-reduction, next (*n*th) cycle starts within a small enzyme fraction $\alpha^n$, which can be neglected. This ensures negligible contribution of multiple turnover of the enzyme.

## Numerical modeling of the complete single turnover kinetics

The dynamics of the system (Scheme 2) can be represented in a reduced form as a linear system of ordinary differential equations:

$$\begin{cases} \dot{x}_1 = -v_1 \\ \dot{x}_2 = v_1 - v_2 \\ \dot{x}_3 = v_2 - v_3 \\ \dot{x}_4 = v_3 \\ \dot{\Delta\psi}_1 = \Psi_1 \times C \times v_1 - v_4 - v_6 \\ \dot{\Delta\psi}_2 = \Psi_2 \times C \times v_2 + v_4 - v_5 - v_7 \\ \dot{\Delta\psi}_3 = \Psi_3 \times C \times v_3 + v_5 - v_8 \end{cases} \tag{5}$$

with the reaction rates

$$\begin{cases} v_1 = k_1^{app} \times x_1 \\ v_2 = k_2^{app} \times x_2 \\ v_3 = k_3^{app} \times x_3 \\ v_4 = k_2^{app} \times \Delta\psi_1 \\ v_5 = k_3^{app} \times \Delta\psi_2 \\ v_6 = k_4 \times \Delta\psi_1 \\ v_7 = k_5 \times \Delta\psi_2 \\ v_8 = k_6 \times \Delta\psi_3 \end{cases}$$

and the initial conditions

$$\begin{cases} x_1(0) = 1 \\ x_2(0) = x_3(0) = x_4(0) = 0 \\ \Delta\psi_1(0) = \Delta\psi_2(0) = \Delta\psi_3(0) = 0 \end{cases}.$$

Here $x_1 \ldots x_4$ are the reduced concentrations of the catalytic states, **R**, $\mathbf{O_H}$, $\mathbf{E_H}$, and $\mathbf{R_1}$, respectively (Scheme 2), so that the total concentration of the enzyme equals 1:

$$\sum_1^4 x_i = 1; \tag{6}$$

$\Delta\psi_1 \ldots \Delta\psi_3$ are the transmembrane potentials [mV] accumulated at the reaction steps (1)… (3), respectively (Scheme 2); $\Psi_{1\ldots3} \times C$ are the stoichiometrical factors quantifying $\Delta\psi$ generated on the consumption of 1 molar unit of reactant at each of the reaction steps (1)… (3), respectively, where there is no loss;

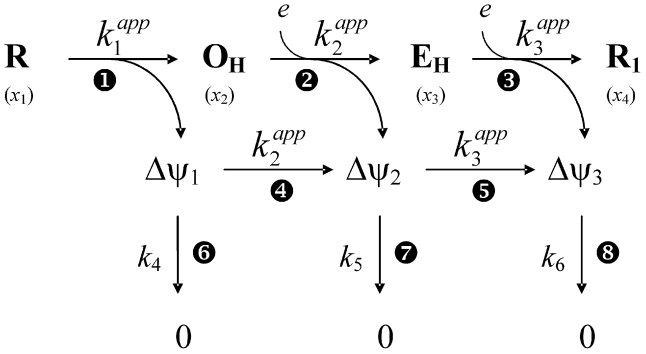


SCHEME 2 Kinetic scheme for the transition between the catalytic states and formation and dissipation of the membrane potential during the catalytic cycle of C*c*O in the complete single turnover experiment. Reaction steps are shown by numbers. Rates constants $k_1^{app}$, $k_2^{app}$, $k_3^{app}$, are defined by Eqs. 1, 7, and 8, respectively. The electron donor is represented as $e^-$. The observed kinetics is defined as $\Delta\psi(t) = \Delta\psi_1(t) + \Delta\psi_2(t) + \Delta\psi_3(t)$.

$\Psi_{1\ldots3}$ are the numbers of equivalent, dielectrically-weighted charges electrogenically transferred within a given C*c*O molecule at each of the reaction steps (1)… (3), respectively; $C$ is a concentration factor to convert number of charges into mV ($\Delta\psi$ produced on the transfer of 1 charge). The apparent rate constants $k_1^{app}$, $k_2^{app}$, $k_3^{app}$, are defined by Eqs. 1, 7, and 8, respectively:

$$k_2^{app} = k_2 \times \left[\mathrm{HAR^{Red}}\right], \tag{7}$$

$$k_3^{app} = k_3 \times \left[\mathrm{HAR^{Red}}\right], \tag{8}$$

where $k_2$ and $k_3$ are the rate constants of the reduction of BNC by an electron donor at the transitions $\mathbf{O_H} \rightarrow \mathbf{E_H}$ and $\mathbf{E_H} \rightarrow \mathbf{R}$, respectively. The concentrations of the reactants (CO and $O_2$ in Eq. 1 and $HAR^{Red}$ in Eqs. 7 and 8) are treated as time-independent parameters.

Because the right-hand parts of the equations for $x_1(t)$ … $x_4(t)$ (Eq. 5) do not depend on $\Delta\psi_1$ … $\Delta\psi_3$, and taking into account a single stoichiometrical rule for the system (Eq. 6), then the first four equations in Eq. 5 can be solved separately giving a simple three-exponential solution, provided that $k_1^{app} \neq k_2^{app} \neq k_3^{app}$ (see Supporting Material):

$$\begin{cases} x_1(t) = e^{-k_1^{app}t} \\ x_2(t) = \dfrac{k_1^{app}}{k_2^{app}-k_1^{app}}\, e^{-k_1^{app}t} + \dfrac{k_1^{app}}{k_1^{app}-k_2^{app}}\, e^{-k_2^{app}t} \\ x_3(t) = \dfrac{k_1^{app}k_2^{app}}{(k_2^{app}-k_1^{app})(k_3^{app}-k_1^{app})}\, e^{-k_1^{app}t} \\ \qquad + \dfrac{k_1^{app}k_2^{app}}{(k_1^{app}-k_2^{app})(k_3^{app}-k_2^{app})}\, e^{-k_2^{app}t} \\ \qquad + \dfrac{k_1^{app}k_2^{app}}{(k_1^{app}-k_3^{app})(k_2^{app}-k_3^{app})}\, e^{-k_3^{app}t} \\ x_4(t) = 1 - \sum_1^3 x_i \end{cases}. \tag{9}$$

Then the total membrane potential generation $\Delta\psi(t) = \sum_1^3 \Delta\psi_i(t)$ that corresponds to the experimentally observed entity can be found from

$$\begin{cases} \dot{\Delta\psi}_1 = \Psi_1 \times C \times k_1^{app} \times x_1(t) - (k_2^{app} + k_4) \times \Delta\psi_1 \\ \dot{\Delta\psi}_2 = \Psi_2 \times C \times k_2^{app} \times x_2(t) + k_2^{app} \times \Delta\psi_1 - (k_3^{app} + k_5) \times \Delta\psi_2 \\ \dot{\Delta\psi}_3 = \Psi_3 \times C \times k_3^{app} \times x_3(t) + k_3^{app} \times \Delta\psi_2 - k_6 \times \Delta\psi_3 \end{cases}, \tag{10}$$

where functions $x_1(t)$ … $x_3(t)$ are obtained in analytical form from Eq. 9. Note that Eq. 10 cannot be further reduced and its exact solution is the sum of six exponentials.

The time-dependences $\Delta\psi(t)$ were evaluated by numerical integration of the system (Eq. 10) using a Runge-Kutta algorythm (the MATLAB function **ode45** was used; The MathWorks, Natick, MA). To fit the solution to the experimentally observed set of data (see Fig. 4), $\Delta\psi(t)$ was evaluated simultaneously at a fixed set of concentrations of the electron donor ($[HAR^{Red}]$) matching the experiment. The values of $[HAR^{Red}]$-dependent constants, $k_2^{app}$ and $k_3^{app}$ (Eqs. 7, 8), were calculated at each concentration point. A set of seven parameters ($k_1^{app}$, $k_2$ … $k_6$, $C$) was used as independent unconstrained variables subject to the optimization for the whole set of $[HAR^{Red}]$ values (Table 1). The values of $\Psi_1$ … $\Psi_3$ (Eq. 5) were partially constrained according to the assumed dielectric distances and the number of transmembrane charges transferred in C*c*O (Table 2 and Fig. 1):

$$\begin{cases} \Psi_1 \approx 3.7(\pm 10\%) \\ \Psi_2 \approx \Psi_3 \approx 0.5 \times 4.3(\pm 10\%) \\ \sum_1^3 \Psi_i = 8 \end{cases}. \tag{11}$$

It has been noted that at concentrations higher than ~10 $\mu$M, $HAR^{Red}$ causes a slight uncoupling effect of the liposome membrane; the effect was clearly concentration-dependent but did not correlate with any other $[HAR^{Red}]$-dependent process observed. Thus the uncoupling was taken into account by assuming an exponential kinetics with $\tau$ linearly dependent on $[HAR^{Red}]$ and subtraction from the whole data sets.

All calculations were carried out using MATLAB (The MathWorks).

## RESULTS

### Generation and relaxation of $\Delta\psi$ in the proteoliposomes with reconstituted C*c*O

The freshly oxidized state $\mathbf{O_H}$ of C*c*O can be obtained by the oxidation of fully reduced enzyme ($\mathbf{R_{FR}}$) with oxygen in the absence of reductant. This leaves the enzyme in state $\mathbf{O_H}$ for a time long enough (>>10 s) to follow $\Delta\psi$ relaxation specifically attributed to this state. When the oxidized enzyme is rapidly re-reduced to form state $\mathbf{R_{FR}}$, $\Delta\psi$ relaxation that follows is much slower than in the former case. We report two experiments that show such difference in the relaxation kinetics.

Fig. 2 shows the $\Delta\psi$ dynamics in C*c*O-proteoliposomes during the flow-flash (Fig. 2, *A* and *C*) and the complete single turnover (Fig. 2 *B*) experiments.

In the flow-flash experiment, C*c*O reacts with oxygen present in high concentration (12,13). After photolysis of

**TABLE 1 Best fit parameters (Eq. 10) for the $\Delta\psi$ generation and relaxation kinetics in C*c*O-proteoliposomes in the complete single turnover experiment**

| | Formation of $\Delta\psi$ accompanying the transitions between the catalytic intermediates | | | Dissipation of $\Delta\psi$ associated with formation of intermediates | | |
|---|---|---|---|---|---|---|
| | $\mathbf{R_{FR}} \rightarrow \mathbf{O_H}$ | $\mathbf{O_H} \rightarrow \mathbf{E_H}$ | $\mathbf{E_H} \rightarrow \mathbf{R_{FR}}$ | $\mathbf{O_H}$ | $\mathbf{E_H}$ | $\mathbf{R_{FR}}$ |
| | $k_1^{app}$, $s^{-1}$ | $k_2 \times 10^6$, $M^{-1}\,s^{-1}$ | $k_3 \times 10^6$, $M^{-1}\,s^{-1}$ | $k_4$, $s^{-1}$ | $k_5$, $s^{-1}$ | $k_6$, $s^{-1}$ |
| *P. denitrificans* wild-type enzyme | 55 ± 3 | 1.7 ± 0.1 | 0.65 ± 0.04 | 1.2 ± 0.1 | 0.30 ± 0.04 | 0.30 ± 0.04 |
| Bovine heart mitochondrial enzyme | 40 | 0.36 ± 0.06 | 0.22 ± 0.08 | 1.4 ± 0.2 | 0.52 ± 0.04 | 0.36 ± 0.03 |

**TABLE 2 Numbers of net electrogenic charges transferred in C*c*O per cycle ($d = 0.3$)**

| $\Psi_1$ | $\Psi_2 + \Psi_3$ | $\frac{\Psi_2 + \Psi_3}{\Psi_1}$ | $\frac{\Delta\psi_{RED}}{\Delta\psi_{OX}}$ | | $\Psi_2$ | $\Psi_3$ |
|---|---|---|---|---|---|---|
| | | | *P. denitrificans* | Bovine | | |
| 3.7 | 4.3 | 1.16 | 1.15 ± 0.02 | 1.18 ± 0.05 | 2.0–2.3* | 2.3–2.0* |

*Shows the limits of the respective $\Psi_i$ values when the electron transfer between $Cu_A$ and heme *a* gets to equilibrium within the time frame of the transitions $\mathbf{O_H} \rightarrow \mathbf{E_H}$ and $\mathbf{E_H} \rightarrow \mathbf{R_{FR}}$, respectively, with the distribution varying from 0 to 1 (Fig. 1).

the C*c*O-CO complex, the whole population of the enzyme reaches the state $\mathbf{O_H}$ within 3–5 ms. The accompanying generation of $\Delta\psi$ is immediately followed by the relaxation phase (Fig. 2 *A*, proteoliposomes with bovine enzyme, $\Delta\psi_{OX}^{100\%} \approx 100$ mV; the rise phase is not resolved in the figure). The major phase of the relaxation shows $\tau =$ 0.5–0.8 s. Typically, incubation with 0.05–0.1 $\mu$M $HAR^{Red}$ for a few minutes is required to re-reduce the enzyme to the initial state $\mathbf{R_{FR}CO}$ so that the re-reduction (or possible multiple turnover) kinetics does not affect the observed $\Delta\psi$ relaxation.

In the complete single turnover experiment, CO and oxygen compete for the binding site in BNC and both binding of CO and reduction of oxygen are rate-limited by the former with $\tau = 15$–25 ms (Eq. 3). Both are electrogenic, although at longer timescales ($t >> 25$ ms) the contribution of photolysis and re-binding of CO ($\Delta\psi_{CO}$) cannot be seen and this does not affect the results (for shorter timescales, the kinetics of re-binding of CO measured separately can be subtracted from the observed $\Delta\psi$ transients to recover the oxygen-induced kinetics; see below). Under the conditions with 60–90 nM $O_2$ ~2% C*c*O binds oxygen producing $\Delta\psi_{OX}^{\alpha} \approx 2$ mV (Fig. 2 *B*, *curve 1*, proteoliposomes with bovine enzyme). In the absence of reductant, the formation of state $\mathbf{O_H}$ is followed by the $\Delta\psi$ relaxation with a major decay component ($\tau =$ 0.4–0.7 s), although minor phases, both faster and slower, can also be seen (*curve 1*). In the presence of reductant, the reductive half-reaction and formation of state $\mathbf{R_{FR}}$ contribute to an additional, slower $\Delta\psi$ rise of a similar amplitude that of the oxidative half-reaction and the $\Delta\psi$ relaxation that follows is even slower ($\tau$ ~1.5 s, Fig. 2 *B*, *curve 2*). Note that to compare the two kinetics, curve 2 was scaled so that its $\Delta\psi$ decay component has the same amplitude (2 mV) as for curve 1. The dashed line (Fig. 2 *B*, *curve 3*) shows the simulated relaxation kinetics with the same concentration of the reductant as in curve 2, but when the $[HAR^{Red}]$-dependent uncoupling effect seen at the concentrations higher than ~10 $\mu$M, was subtracted.

Comparison between Fig. 2, *A* and *B*, *curve 1*, makes it clear that 1), the $\Delta\psi$ relaxation kinetics are similar, despite the 50× difference in the amplitude and the fact that the state $\mathbf{O_H}$ was prepared differently; and 2), when the state $\mathbf{O_H}$ is converted rapidly to $\mathbf{R_{FR}}$, the $\Delta\psi$ dissipation kinetics becomes much slower (Fig. 2, *curves 1* and *2*). Similar results were obtained with wild-type *Paracoccus* enzyme showing rapid $\Delta\psi$ relaxation after the oxidative phase both in the flow-flash experiment (Fig. 2 *C*, *WT*) and in the complete single turnover experiment in the absence of an external reductant (data not shown; in both cases the major component of the decay has $\tau \approx 0.5$ s) but significantly slower $\Delta\psi$ relaxation ($\tau \geq 2.5$ s) in the complete single turnover experiment when $[HAR^{Red}] > 20$ $\mu$M was present (data not shown). We proposed that at least two relaxation processes with different time constants are involved in the $\Delta\psi$ relaxation in C*c*O-proteoliposomes. Although the slower component of $\Delta\psi$ decay can be rate-limited by unspecific enzyme- or membrane-mediated dissipation, the faster one is due to the specific proton leak through the enzyme at the certain state of its catalytic cycle.

The structure of C*c*O (28,29) identifies two distinct input proton-conducting channels leading from N-side of the membrane to the catalytic domain of the enzyme: 1), D-channel serves as the proton input for both proton pumping and proton delivery to BNC for the chemical reaction, except that the latter proceeds only during the oxidative half-reaction; and 2), K-channel is responsible only for proton delivery to BNC during the reductive half-reaction (30,31). It is likely that the elevated proton leak proceeds through one of these channels. To test this possibility we repeated the flow-flash experiment, above, with the enzyme where the proton transfer along the either one of these channels was specifically blocked (30,32) (D124N, in D-channel, and K354M, in K-channel; amino acid residue numbering as for Subunit I of *P. denitrificans* $aa_3$-type C*c*O). Fig. 2 *C* shows that $\Delta\psi$ relaxation kinetics in K354M enzyme is almost as fast as in WT. However, with D124N enzyme the decay is at least five times slower (the major decay phase is one-exponential with $\tau \approx 3$ s, thin dashed line), despite the fact that the $\Delta\psi$ generation and $\mathbf{O_H}$ formation (33) in this mutant has also been slowed down.

## Complete single turnover kinetics of C*c*O: measurement and modeling

The data shown above cannot tell about the specific $\Delta\psi$ relaxation kinetics involving the one-electron reduced state $\mathbf{E_H}$. Indeed, in the two-step reaction $\mathbf{O_H} \rightarrow \mathbf{E_H} \rightarrow \mathbf{R_{FR}}$, which takes place in the presence of reductant, it is only possible to trap the state $\mathbf{E_H}$ transiently before it converts to $\mathbf{R_{FR}}$. Thus, measuring the $\Delta\psi$ kinetics at different $[HAR^{Red}]$ and numerical modeling were required to distinguish between state $\mathbf{E_H}$-specific $\Delta\psi$ relaxation and other processes. Fig. 3 shows $\Delta\psi$ generation in C*c*O-proteoliposomes in the

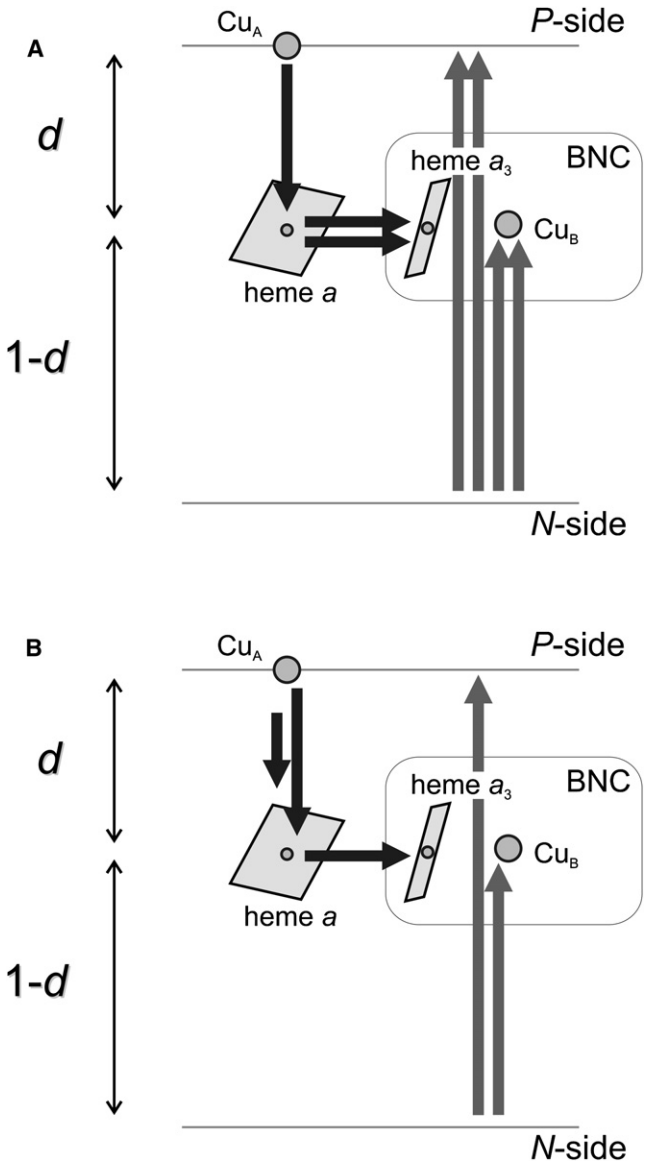


FIGURE 1 Stoichiometry of the net electrogenic charge transfer in C*c*O. (*A*) Oxidative phase ($\mathbf{R_{FR}} \rightarrow \mathbf{O_H}$). (*B*) Reductive phase (one-electron reduction step shown, $\mathbf{O_H} \rightarrow \mathbf{E_H}$ and $\mathbf{E_H} \rightarrow \mathbf{R_{FR}}$). Arrows in black are electron transfer; arrows in gray are proton transfer. The dielectric thickness of the whole membrane domain is taken as 1. The dielectric depth (distance from the membrane N-side) at which heme *a* and BNC are located, is taken as $d$ ($0 < d < 1$). Taking $d = 0.3$, the numbers of net charges transferred are (*A*) $\Psi_1 = 3.7$, and (*B*) $\Psi_2 \approx \Psi_3 \approx 4.3/2$.

complete single turnover experiment, similar to Fig. 2 *B*, but with *Paracoccus* enzyme, recorded on a shorter timescale, and at different concentrations of reductant. The kinetics is a superposition of the oxidative phase ($\Delta\psi^{\alpha}_{OX}$, ~2 mV) in a small fraction of the enzyme population and the photolysis and recombination of CO ($\Delta\psi_{CO}$) in the rest of the enzyme (Fig. 3 *A*). In a separate experiment, when oxygen was totally exhausted by GO at very high concentration, only $\Delta\psi_{CO}$ is observed and can be subtracted from the original data to obtain the pure oxidation and reduction kinetics (Fig. 3 *B*). The increase in the concentration of the reductant leads to the faster repopulation of the state $\mathbf{R_{FR}}$ and causes the appearance of reductive phase ($\Delta\psi^{\alpha}_{RED}$) that can be extrapolated to ~2.3 mV taking into account both the dependence of the total $\Delta\psi$ on [HAR$^{Red}$] and the kinetics of $\Delta\psi$ dissipation (Fig. 3 *B*, *dashed line*). Then with $\Delta\psi^{\alpha}_{OX} \approx 2$ mV, the data define the experimental ratio $\Delta\psi_{RED}/\Delta\psi_{OX} \approx 2.3/2 = 1.15 \pm 0.2$. Similar data were obtained with the bovine C*c*O-proteoliposomes (Table 2). The obtained ratios were used as parameters describing the charge transfer stoichiometry within C*c*O for $\Delta\psi$ kinetics modeling.

To quantitate the $\Delta\psi$ kinetics in the single turnover experiment (Scheme 2) one should take into account that because the proteoliposomes used in the study contain only a few C*c*O molecules per liposome ($\leq$4–5, A. Jasaitis and M.I. Verkhovsky, unpublished results; see also Rigaud et al. (23) and Cvetkov et al. (34)) and only a small fraction of the enzyme population reacts with $O_2$ ($\alpha \leq 0.05$), then the probability for more than one enzyme molecule in every given liposome to react with oxygen is negligible; thus, either one or none enters the cycle. Therefore, the $\Delta\psi$ kinetics is independent of the presence of nonreacting (silent) C*c*O molecules in every given liposome. For example, $\Delta\psi_1$ (Scheme 2), once formed, can dissipate only when $\mathbf{O_H}$, $\mathbf{E_H}$, or $\mathbf{R_1}$, are formed. Similarly, $\Delta\psi_2$ dissipates at the states $\mathbf{E_H}$ or $\mathbf{R_1}$ and $\Delta\psi_3$ dissipates when $\mathbf{R_1}$ is formed. The fraction of the silent C*c*O, originally in the state $\mathbf{R_{FR}CO}$, re-binds CO after the flash, but its kinetics coincides with that of the oxidative phase in the active fraction (Eq. 3), so it will not affect any slower $\Delta\psi$ relaxation. We further introduce specific rates of $\Delta\psi$ dissipation, $k_4$, $k_5$, $k_6$, at the states $\mathbf{O_H}$, $\mathbf{E_H}$, and $\mathbf{R_1}$, respectively (reactions (6)… (8), Scheme 2). We further assume that $\Delta\psi$ dissipation at any given step is of a simple 1st-order kinetics and that all steps in Scheme 2 are irreversible and, therefore, the formation of $\Delta\psi$ has itself no effect on the observed rate constants.

The measured $\Delta\psi$ kinetics together with the results of its numerical fit are shown on Fig. 4. It is clear that 1), at low [HAR$^{Red}$] (<0.6 $\mu$M, *Paracoccus* C*c*O, Fig. 4 *A*) fast relaxation ($\tau << 1$ s) prevails and the $\Delta\psi_{RED}$ generation phase cannot be seen; 2), at [HAR$^{Red}$] $\approx$ 1 $\mu$M there is an interplay between the fast relaxation and slightly slower generation phase followed by a yet slower relaxation; and 3), at high [HAR$^{Red}$] (>2 $\mu$M) the fast relaxation is no longer observed; instead, the $\Delta\psi_{RED}$ generation phase followed by the slow relaxation is seen. With bovine C*c*O, similar results are obtained (Fig. 4 *B*), except that ~5-fold higher concentrations of HAR$^{Red}$ were required to produce equivalent data. The values of rate constants obtained by the fitting are summarized in Table 1. The values of $k_1^{app}$ are close to the published values for the rate of CO recombination (Fig. 3 *A*, *dashed line*). The re-reduction of BNC proceeds in two successive steps; for both *Paracoccus* and bovine enzymes the values of $k_2^{app}$ ($\mathbf{O_H} \rightarrow \mathbf{E_H}$) were three to four times higher than of $k_3^{app}$ ($\mathbf{E_H} \rightarrow \mathbf{R_{FR}}$). There is not much difference between

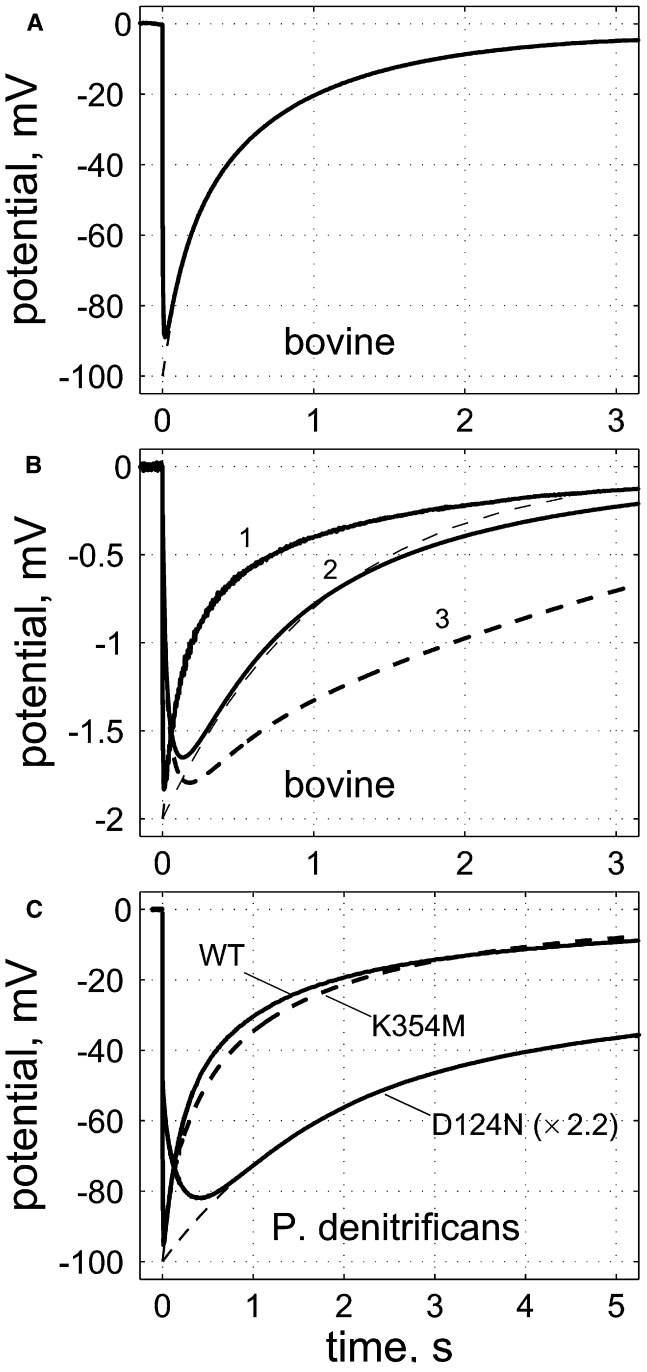


FIGURE 2 Generation and decay of $\Delta\psi$ in C*c*O-proteoliposomes. (*A*) Bovine C*c*O, electrometric flow-flash experiment. (*B*) Same enzyme as in *A*, but in the electrometric complete single turnover experiment. In *B*, $[HAR^{Red}] = 0.1$ $\mu$M (*curve 1*) and 100 $\mu$M (*curves 2 and 3*). Curve 3 is the same as curve 2 but with the uncoupling effect of $HAR^{Red}$ subtracted. Thin dashed line shows a one-exponential approximation of curve 2 extrapolated to $\Delta\psi = 2$ mV at $t = 0$. (*C*) Same experiment as in *A*, but with *Paracoccus* wild-type (WT), and the K254M and D124N mutant enzymes. Conditions: 100 mM EPPS (pH 8.1), 100 mM D-glucose, 0.2 mg/mL catalase, ~100% CO atmosphere. In *A* and *C*, 200 U/mL GO is present. In *B*, 16 U/mL GO is present. In *B*, 0.1% (v/v) air is present in the gas phase maintaining ~60–90 nM $O_2$ in solution. Both bovine and *Paracoccus* C*c*O-proteoliposomes contained 7 $\mu$M enzyme. A laser flash initiated the photolysis of C*c*O-CO complex and started data acquisition ($t = 0$). All transients are normalized so that the absolute values of the total amplitude of their $\Delta\psi$ decay phase are (*A*, C) 100 mV, or (*B*) 2 mV. The actual amplitudes with the same proteoliposome preparations ranged from 80 to 120 mV (*A* and *C*, WT and K354M), 30–50 mV (*C*, D124N), and (*B*) 1–5 mV .

the slower phases of $\Delta\psi$ dissipation ($k_5$, $k_6$), so they may describe the C*c*O-unspecific $\Delta\psi$ dissipation. However, the value of $k_4$ (relaxation when C*c*O is in the state $\mathbf{O_H}$) is four to five times higher than $k_5$ and $k_6$ and close to the $\Delta\psi$ decay rate constant obtained in the flow-flash experiment, where the same relaxation step is observed. Thus the behavior of the reductant-dependent $\Delta\psi$ kinetics is consistent with the proposed model involving two relaxation processes.

## DISCUSSION

### Complete single turnover of C*c*O: the idea of the experiment

Tracking $\Delta\psi$ generation by C*c*O during either the oxidative or reductive phases of the catalytic cycle can be achieved separately in different experiments by means of flow-flash (12,13) or electron injection techniques (7,35–37), as reported earlier. Observation of the oxidative phase requires that the reductant present in a very small quantity to prevent rapid re-reduction and oxygen be added at high concentration so that its binding is not a limiting factor. Conversely, re-reduction of the oxidized enzyme requires high concentration of the reductant and lack of oxygen. When the reductant and oxygen are both present at large concentration, the enzyme will enter the multiple turnover regime preventing the observation a synchronized turnover. We have developed a procedure that allows one to track $\Delta\psi$ during both oxidative and reductive phases in one experiment, which has been described briefly in Verkhovsky et al. (6). To achieve such conditions a very low (~0.02–0.2 $\mu$M) steady-state concentration of oxygen is maintained by the balance between the oxygen influx from the gas phase into the solution and its depletion by the glucose-GO-catalase enzymatic system (Supporting Material). In the presence of CO and reductant C*c*O is trapped in the fully reduced state with CO bound to the binuclear site ($\mathbf{R_{FR}CO}$). Photolysis of the $\mathbf{R_{FR}CO}$ enzyme with a short laser flash yields reduced, unliganded enzyme ($\mathbf{R_{FR}}$) that can bind ether CO or oxygen. Most of the population of the enzyme (fraction 1-$\alpha$, Scheme 1) binds CO and returns back to the $\mathbf{R_{FR}CO}$ state, whereas a small fraction ($\alpha$) reacts with oxygen progressing through the oxidative phase ($\Delta\psi_{OX}$) and then (in the presence of reductant) slower reductive phase ($\Delta\psi_{RED}$). After the reaction is complete, the fraction $\alpha$ of the enzyme has again the choice either to bind CO or react with oxygen and proceed through the next cycle. However, this is only fraction $\alpha$ (2%–5%) of the obtained signal that will be added up to a slow phase and can be either neglected or subtracted from the kinetics. This ensures that only one turnover of the enzyme is observed.

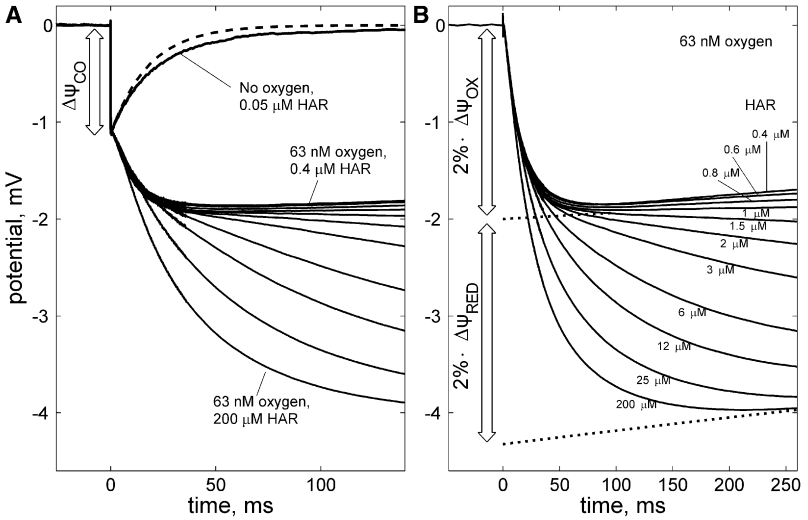


FIGURE 3 Generation of $\Delta\psi$ in the complete single turnover experiment with *P. denitrificans* C*c*O-proteoliposomes. (*A*) Transients after CO photolysis (laser flash instance is at $t = 0$). CO-recombination kinetics ($\mathbf{R_{FR}} \rightarrow \mathbf{R_{FR}CO}$) is shown as the curve in the absence of oxygen. Other curves are in the presence of 63 nM $O_2$ and at various concentration of reductant. (*B*) Same as *A*, but after subtraction of the CO-recombination kinetics. In *A*, dashed line is the simulated mono-exponential kinetics of the oxidative phase with $k_1^{app} = 55\ s^{-1}$ (Table 1). In *B*, dotted lines are the extrapolation of the oxidative phase and the total voltage to $t = 0$. Arrows indicate voltage associated with the oxidative and reductive phases of the catalytic cycle ($\alpha = 0.02$) and re-binding of CO ($1 - \alpha = 0.98$). Other conditions: as for Fig. 2.

## Oxidative and reductive parts of C*c*O cycle

Although generation of $\Delta\psi_{OX}$ is reductant-independent (Eqs. 1 and 3), the kinetics of $\Delta\psi_{RED}$ varies with the amount of reductant (Eqs. 7 and 8). At $[HAR^{Red}] \leq 3\ \mu M$ (*Paracoccus* enzyme) oxidative and reductive phases are kinetically well-separated, which allows one to determine the amplitude of $\Delta\psi_{OX}$. At higher $[HAR^{Red}]$, their kinetics merge and the total amplitude ($\Delta\psi_{OX} + \Delta\psi_{RED}$) can be found (Fig. 3 *B*). Importantly, the $\Delta\psi$ relaxation that follows significantly affects the observed $\Delta\psi$ generation kinetics and should be taken into account for further quantitative analysis.

Generally, the maximum $\Delta\psi$ amplitude is proportional to the dielectrically weighted distance that a charge travels perpendicularly to the membrane plane and to the number of net charges transferred. During the oxidative phase (Fig. 1 *A*) two electrons to reduce oxygen are taken from within BNC and two other are provided by the prereduced heme *a* and $Cu_A$. Here the only significantly electrogenic step is the electron transfer from $Cu_A$ to heme *a*, which contributes to the transfer of one charge at the dielectric distance *d*. However, two pumped protons are also translocated through the whole membrane (dielectric distance = 1) and two more, chemical protons are taken up to the BNC (dielectric distance = $1 - d$), which makes the number of the electrogenically transferred net charges $\Psi_1 = 2 + 2 \times (1 - d) + d = 4 - d$. During the reductive phase (Fig. 1 *B*) BNC, heme *a*, and $Cu_A$, are re-reduced by four electrons from an external reductant. Each of the two electrons entering BNC (transitions $\mathbf{O_H} \rightarrow \mathbf{E_H}$ and $\mathbf{E_H} \rightarrow \mathbf{R_{FR}}$) causes the same protonic phase (one pumped and one chemical proton) and the $Cu_A$ to heme *a* electron transfer making stoichiometry of two charges per one electron. The electrogenic re-reduction of heme *a* also contributes to the reductive phase; thus, $\Psi_2 + \Psi_3 = 4 + d$. Because re-reduction of heme *a* and any of the redox reactions in BNC are kinetically not coupled, the small electrogenic phase of heme *a* reduction is distributed between $\Psi_2$ and $\Psi_3$. From the x-ray structure

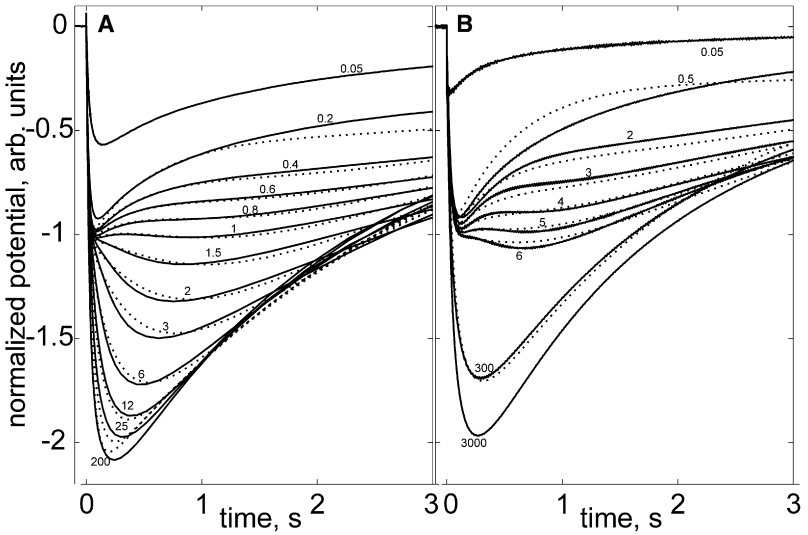


FIGURE 4 Modeling the $\Delta\psi$ generation and decay in the complete single turnover experiment. (*A*) *P. denitrificans* C*c*O-proteoliposomes. (*B*) Bovine heart mitochondrial C*c*O-proteoliposomes. Data curves are shown as solid lines; simulated curves are shown as dotted lines. Numbers at the curves indicate $[HAR^{Red}]$, $\mu$M. All curves are obtained after subtraction of the CO-recombination kinetics (Fig. 3) and are shown without further normalization. Conditions as for Fig. 2. The uncoupling effect of $HAR^{Red}$ was subtracted. Simulated curves are plotted according to the best fit solutions (Eq. 10) with parameters listed in Tables 1 and 2.

(28,29), the geometrical projection of the distance between the *P*-side of the membrane and BNC is about one third of the membrane thickness. Also from our earlier $\Delta\psi$ kinetic measurements (13), $d$ was found ~0.3, which gives $\Psi_1 = 3.7$ and $\Psi_2 + \Psi_3 = 4.3$ (Table 2) and the ratio between the amplitudes of reductive versus oxidative phases $(\Psi_2 + \Psi_3)\Psi_1 \approx 1.16$. The experimental values for this ratio (Table 2) are indeed in a very good quantitative agreement with the prediction.

Modeling also shows a difference between the rate constants of the 1st ($k_2$) and 2nd ($k_3$) electron delivery to the oxidized, and $\mathbf{E_H}$-state, BNC, respectively, making the $\Delta\psi_{RED}$ kinetics biphasic. However, the observed difference is not enough large ($\leq$5 times) to separate the two electrogenic steps. Therefore, $\Psi_2$ and $\Psi_3$ cannot be separately determined from the experiment (Table 2 shows hypothetical limits for their values assuming the electron distribution between $Cu_A$ and heme *a* varying from 0 to 1).

### Relaxation of $\Delta\psi$ in C*c*O-proteoliposomes

In the electrometry setup, the effective resistance and capacitance of the measuring film are typically 0.5–1 $\times$ $10^8$ Ohm $\times$ $cm^2$ and 0.2–0.3 $\mu F/cm^2$, respectively, giving the characteristic $\tau$ of 10–30 s. This sets an upper limit for the $\tau$ determination in any observed $\Delta\psi$ kinetics. In this study, the slowest $\Delta\psi$ relaxation kinetics has $\tau \approx 3$ s both for bovine and *Paracoccus* enzymes. Because in the complete single turnover experiment each liposome contains several silent $\mathbf{R_{FR}}$-state C*c*O molecules, we believe that the $\tau \approx 3$ s relaxation is related either with the lipid itself or with the $\mathbf{R_{FR}}$-state enzyme. The presence of a faster ($\tau < 0.8$ s) relaxation phase immediately after oxidation imposes that the state $\mathbf{O_H}$ differs from states $\mathbf{E_H}$ and $\mathbf{R_{FR}}$ and provides an internal way for proton leak.

K-channel is known to be involved only in the re-reduction of C*c*O but not in the oxidation. This is in line with the data that the kinetics of the formation of state $\mathbf{O_H}$ tracked optically in the K-channel mutant (K354M) and in WT enzymes are very similar (38). Indeed, we show that in the mutant the $\Delta\psi$ relaxation after rapid formation of $\mathbf{O_H}$ does not differ from that in WT ($\tau \approx$ 0.5–0.7 s). Conversely, block in the D-pathway (D124N) leads to the loss of proton pumping at the oxidative phase, though leaving chemical transitions of BNC nearly intact (31). In the D124N mutant the fast $\Delta\psi$ relaxation through the $\mathbf{O_H}$-state enzyme is no longer observed. We conclude that the proton conductance through the D-channel in the $\mathbf{O_H}$-state WT or K354M enzyme may itself provide the $\tau \approx$ 0.5–0.7 s relaxation kinetics, whereas its block eliminates such fast relaxation. It is plausible that C*c*O can provide ways for the leak through their proton pump machinery either by the partial reversal of its function or by slipping or uncoupling between electron and proton transport (39).

## SUPPORTING MATERIAL

Three equations and one scheme are available at http://www.biophysj.org/biophysj/supplemental/S0006-3495(09)00696-1.

This work was supported by Biocentrum Helsinki (project number 7919028), Sigrid Jusélius Foundation (project number 4700827 and Research Fellowship to D.A.B.), Magnus Ehrnrooth Foundation (research grant to D.A.B.), and the Academy of Finland (project number 115108).

## REFERENCES

1. Mitchell, P. 1961. Coupling of phosphorylation to electron and hydrogen transfer by a chemi-osmotic type of mechanism. *Nature*. 191:144–148.
2. Mitchell, P. 1976. Possible molecular mechanisms of the proton motive function of cytochrome systems. *J. Theor. Biol.* 62:327–367.
3. Wikström, M. K. 1977. Proton pump coupled to cytochrome *c* oxidase in mitochondria. *Nature*. 266:271–273.
4. Babcock, G. T., and M. Wikström. 1992. Oxygen activation and the conservation of energy in cell respiration. *Nature*. 356:301–309.
5. Belevich, I., and M. I. Verkhovsky. 2008. Molecular mechanism of proton translocation by cytochrome *c* oxidase. *Antioxid. Redox Signal.* 10:1–29.
6. Verkhovsky, M. I., A. Jasaitis, M. L. Verkhovskaya, J. E. Morgan, and M. Wikström. 1999. Proton translocation by cytochrome *c* oxidase. *Nature*. 400:480–483.
7. Bloch, D., I. Belevich, A. Jasaitis, C. Ribacka, A. Puustinen, et al. 2004. The catalytic cycle of cytochrome *c* oxidase is not the sum of its two halves. *Proc. Natl. Acad. Sci. USA*. 101:529–533.
8. Verkhovsky, M. I., I. Belevich, D. A. Bloch, and M. Wikström. 2006. Elementary steps of proton translocation in the catalytic cycle of cytochrome oxidase. *Biochim. Biophys. Acta*. 1757:401–407.
9. Wikström, M., and M. I. Verkhovsky. 2007. Mechanism and energetics of proton translocation by the respiratory heme-copper oxidases. *Biochim. Biophys. Acta*. 1767:1200–1214.
10. Drachev, L. A., A. A. Jasaitis, A. D. Kaulen, A. A. Kondrashin, E. A. Liberman, et al. 1974. Direct measurement of electric current generation by cytochrome oxidase, $H^+$-ATPase and bacteriorhodopsin. *Nature*. 249:321–324.
11. Drachev, L. A., A. D. Kaulen, A. Y. Semenov, I. I. Severina, and V. P. Skulachev. 1979. Lipid-impregnated filters as a tool for studying the electric current-generating proteins. *Anal. Biochem.* 96:250–262.
12. Verkhovsky, M. I., J. E. Morgan, M. L. Verkhovskaya, and M. Wikström. 1997. Translocation of electrical charge during a single turnover of cytochrome *c* oxidase. *Biochim. Biophys. Acta*. 1318:6–10.
13. Jasaitis, A., M. I. Verkhovsky, J. E. Morgan, M. L. Verkhovskaya, and M. Wikström. 1999. Assignment and charge translocation stoichiometries of the major electrogenic phases in the reaction of cytochrome *c* oxidase with dioxygen. *Biochemistry*. 38:2697–2706.
14. Chernomordik, L., M. M. Kozlov, and J. Zimmerberg. 1995. Lipids in biological membrane fusion. *J. Membr. Biol.* 146:1–14.
15. Stegmann, T., J. Teissie, and M. Winterhalter. 2001. Fusion and rupture of lipid model membranes. *In* Lipid Bilayers: Structure and Interactions. J. Katsaras and T. Gutberlet, editors. Springer-Verlag, Berlin, pp. 265–287.
16. Hendler, R. W., L. A. Drachev, S. Bose, and M. K. Joshi. 2000. On the kinetics of voltage formation in purple membranes of *Halobacterium salinarum*. *Eur. J. Biochem.* 267:5879–5890.
17. Schönfeld, M., M. Montal, and G. Feher. 1979. Functional reconstitution of photosynthetic reaction centers in planar lipid bilayers. *Proc. Natl. Acad. Sci. USA*. 76:6351–6355.
18. Gopher, A., Y. Blatt, M. Schönfeld, M. Y. Okamura, G. Feher, et al. 1985. The effect of an applied electric field on the charge recombination kinetics in reaction centers reconstituted in planar lipid bilayers. *Biophys. J.* 48:311–320.

19. Riistama, S., A. Puustinen, M. I. Verkhovsky, J. E. Morgan, and M. Wikström. 2000. Binding of $O_2$ and its reduction are both retarded by replacement of valine 279 by isoleucine in cytochrome *c* oxidase from *Paracoccus denitrificans*. *Biochemistry*. 39:6365–6372.

20. Hartzell, C. R., and H. Beinert. 1974. Components of cytochrome c oxidase detectable by EPR spectroscopy. *Biochim. Biophys. Acta*. 368:318–338.

21. Riistama, S., L. Laakkonen, M. Wikström, M. I. Verkhovsky, and A. Puustinen. 1999. The calcium binding site in cytochrome $aa_3$ from *Paracoccus denitrificans*. *Biochemistry*. 38:10670–10677.

22. Ribacka, C., M. I. Verkhovsky, I. Belevich, D. A. Bloch, A. Puustinen, et al. 2005. An elementary reaction step of the proton pump is revealed by mutation of tryptophan-164 to phenylalanine in cytochrome *c* oxidase from *Paracoccus denitrificans*. *Biochemistry*. 44:16502–16512.

23. Rigaud, J. L., B. Pitard, and D. Levy. 1995. Reconstitution of membrane proteins into liposomes: application to energy-transducing membrane proteins. *Biochim. Biophys. Acta*. 1231:223–246.

24. Belevich, I., A. Tuukkanen, M. Wikström, and M. I. Verkhovsky. 2006. Proton-coupled electron equilibrium in soluble and membrane-bound cytochrome *c* oxidase from *Paracoccus denitrificans*. *Biochemistry*. 45:4000–4006.

25. Orii, Y. 1984. Formation and decay of the primary oxygen compound of cytochrome oxidase at room temperature as observed by stopped flow, laser flash photolysis and rapid scanning. *J. Biol. Chem.* 259:7187–7190.

26. Orii, Y. 1988. Intermediates in the reaction of reduced cytochrome oxidase with dioxygen. *Ann. N.Y. Acad. Sci.* 550:105–117.

27. Gibson, Q. H., and C. Greenwood. 1963. Reactions of cytochrome oxidase with oxygen and carbon monoxide. *Biochem. J.* 86:541–544.

28. Iwata, S., C. Ostermeier, B. Ludwig, and H. Michel. 1995. Structure at 2.8 Å resolution of cytochrome *c* oxidase from *Paracoccus denitrificans*. *Nature*. 376:660–669.

29. Tsukihara, T., H. Aoyama, E. Yamashita, T. Tomizaki, H. Yamaguchi, et al. 1995. Structures of metal sites of oxidized bovine heart cytochrome *c* oxidase at 2.8 Å. *Science*. 269:1069–1074.

30. Konstantinov, A. A., S. Siletsky, D. Mitchell, A. Kaulen, and R. B. Gennis. 1997. The roles of the two proton input channels in cytochrome *c* oxidase from *Rhodobacter sphaeroides* probed by the effects of site-directed mutations on time-resolved electrogenic intraprotein proton transfer. *Proc. Natl. Acad. Sci. USA*. 94:9085–9090.

31. Wikström, M., A. Jasaitis, C. Backgren, A. Puustinen, and M. I. Verkhovsky. 2000. The role of the D- and K-pathways of proton transfer in the function of the haem-copper oxidases. *Biochim. Biophys. Acta*. 1459:514–520.

32. Thomas, J. W., A. Puustinen, J. O. Alben, R. B. Gennis, and M. Wikström. 1993. Substitution of asparagine for aspartate-135 in subunit I of the cytochrome *bo* ubiquinol oxidase of *Escherichia coli* eliminates proton-pumping activity. *Biochemistry*. 32:10923–10928.

33. Gorbikova, E. A., N. P. Belevich, M. Wikström, and M. I. Verkhovsky. 2007. Time-resolved ATR-FTIR spectroscopy of the oxygen reaction in the D124N mutant of cytochrome *c* oxidase from *Paracoccus denitrificans*. *Biochemistry*. 46:13141–13148.

34. Cvetkov, T. L., and L. J. Prochaska. 2007. Biophysical and biochemical characterization of reconstituted and purified *Rhodobacter sphaeroides* cytochrome *c* oxidase in phospholipid vesicles sheds insight into its functional oligomeric structure. *Protein Expr. Purif.* 56:189–196.

35. Zaslavsky, D., A. D. Kaulen, I. A. Smirnova, T. Vygodina, and A. A. Konstantinov. 1993. Flash-induced membrane potential generation by cytochrome *c* oxidase. *FEBS Lett.* 336:389–393.

36. Ruitenberg, M., A. Kannt, E. Bamberg, B. Ludwig, H. Michel, et al. 2000. Single-electron reduction of the oxidized state is coupled to proton uptake via the K pathway in *Paracoccus denitrificans* cytochrome *c* oxidase. *Proc. Natl. Acad. Sci. USA*. 97:4632–4636.

37. Verkhovsky, M. I., A. Tuukkanen, C. Backgren, A. Puustinen, and M. Wikström. 2001. Charge translocation coupled to electron injection into oxidized cytochrome *c* oxidase from *Paracoccus denitrificans*. *Biochemistry*. 40:7077–7083.

38. Ädelroth, P., R. B. Gennis, and P. Brzezinski. 1998. Role of the pathway through K(I-362) in proton transfer in cytochrome *c* oxidase from. *R. sphaeroides*. *Biochemistry*. 37:2470–2476.

39. Kaila, V. R., M. I. Verkhovsky, G. Hummer, and M. Wikström. 2008. Glutamic acid 242 is a valve in the proton pump of cytochrome *c* oxidase. *Proc. Natl. Acad. Sci. USA*. 105:6255–6259.